ARTICLE

ACS chemical biology

# Development of Near-Infrared Fluorophore (NIRF)-Labeled Activity-Based Probes for *in Vivo* Imaging of Legumain

**Jiyoun Lee and Matthew Bogyo***

Departments of Pathology and Microbiology and Immunology, Stanford University School of Medicine, 300 Pasteur Dr., Stanford, California 94305-5324

**ABSTRACT** Asparaginyl endopeptidase, or legumain, is a lysosomal cysteine protease that was originally identified in plants and later found to be involved in antigen presentation in higher eukaryotes. Legumain is also up-regulated in a number of human cancers, and recent studies suggest that it may play important functional roles in the process of tumorigenesis. However, detailed functional studies in relevant animal models of human disease have been hindered by the lack of suitably selective small molecule inhibitors and imaging reagents. Here we present the design, optimization, and *in vivo* application of fluorescently labeled activity-based probes (ABPs) for legumain. We demonstrate that optimized aza-peptidyl Asn epoxides are highly selective and potent inhibitors that can be readily converted into near-infrared fluorophore-labeled ABPs for whole body, noninvasive imaging applications. We show that these probes specifically label legumain in various normal tissues as well as in solid tumors when applied *in vivo*. Interestingly, addition of cell-penetrating peptides to the probes enhanced cellular uptake but resulted in increased cross-reactivity toward other lysosomal proteases as the result of their accumulation in lysosomes. Overall, we find that aza-peptidyl Asn ABPs are valuable new tools for the future study of legumain function in more complex models of human disease.

Asparaginyl endopeptidase, also known as legumain, is a lysosomal cysteine protease that was named on the basis of its propensity to cleave protein substrates on the C-terminal side of asparagine residues (*1*). Legumain is expressed in diverse cell types, and in most cases, its functions are unknown. Recently legumain has emerged as an important enzyme in antigen processing (*2, 3*) and matrix degradation (*4, 5*), and it is implicated in various pathological conditions including parasite infection (*6, 7*), atherosclerosis (*8*), and tumorigenesis (*9, 10*). For example, legumain is heavily overexpressed in the majority of human solid tumors such as carcinomas of the breast, colon, and prostate (*9*). Furthermore, knockdown of legumain in mouse models of cancer resulted in a marked decrease in tumor growth and metastasis (*10*). More recently, mice lacking legumain developed disorders similar to hemophagocytic syndrome, a form of hyperinflammatory response (*11*). Despite the mounting evidence of legumain as a therapeutically important target, especially in tumor progression and metastasis, current methods to study legumain function mainly depend on antibodies and genetic modification, making it difficult to study legumain in its native state.

Small molecule chemical tools such as activity-based probes (ABPs) provide a highly versatile means to monitor protease function and regulation in a wide range of biological systems. Typical ABPs utilize irreversible inhibitors that can covalently modify the active site of an enzyme in an activity-dependent fashion. However, only a few legumain-specific inhibitors have appeared in the literature thus far. All of these inhibitors have a Cbz-Ala-Ala-Asn peptide scaffold that is based on the sequence of a known substrate of legumain (*12*). In addi-

*Corresponding author, mbogyo@stanford.edu.

Received for review November 9, 2009 and accepted December 17, 2009.

Published online December 17, 2009

10.1021/cb900232a

tion, a number of different reactive electrophilic functional groups including aza-Asn halomethylketones (*13*), aza-Asn epoxides (*7*), and aza-Asn Michael acceptors (*6*) have been used to make irreversible legumain inhibitors. Although these inhibitors are highly potent against legumain *in vitro*, their potency and, more importantly, their selectivity *in vivo* have never been tested. We have previously developed a cell-permeable ABP for legumain that is composed of a peptide acyloxymethyl ketone (AOMK) with a P1 aspartic acid (*14*). Although this probe is useful to study active legumain in cells, it has overall poor potency and can readily cross-react with caspases, which also optimally bind to aspartic acid containing AOMKs (*15*). We therefore decided to develop a new class of legumain inhibitors with faster kinetic properties and increased selectivity for legumain for use in *in vivo* imaging studies. Herein, we present a new class of aza-Asn epoxide ABPs for legumain that are labeled with Cy5 fluorophore and also tagged with a series of cell-permeabilizing groups. This new generation of legumain probes can be used to image active legumain both in normal tissues and within solid tumors.

## RESULTS AND DISCUSSION

**Design of Legumain Probes for *in Vivo* Applications.** To develop new tools to study legumain function *in vivo*, we needed to identify a scaffold that could be used to make probes that were highly selective for legumain with virtually no cross-reactivity for other lysosomal proteases or related CD clan proteases such as caspases. In the past, our group developed activity-based probes that can be used to label legumain in cell culture models (*14*). These first generation probes make use of the acyloxymethyl ketone (AOMK) group to covalently modify the active site cysteine and a Pro-Asp peptide for specific recognition by legumain. This peptide sequence was chosen on the basis of the finding that although legumain prefers processing of substrates at asparagine residues, it also binds to probes with a P1 aspartic acid (*16*). Since P1 Asn AOMKs are highly unstable (*17*), we originally focused our attention on the P1 Asp AOMK probes. These reagents, while useful for labeling legumain, have overall slow binding properties and generally low potency. In addition, P1 Asp-AOMKs are highly effective labels of caspases both *in vitro* and *in vivo* (*18, 19*). Recent reports suggest that aza-peptidyl epoxides can be designed to be highly potent inhibitors of legumain with overall low cross-reactivity toward other lysosomal cystein proteases such as the cathepsins (*7*). The unique aza scaffold also allows incorporation of a P1 Asn residue without causing overall instability of the compound. On the basis of these findings, we envisioned that aza-Asn epoxide should be valuable for use in imaging probes as a result of very low reactivity toward cathepsins and caspases. We therefore synthesized an activity-based probe LP-1 (Legumain Probe-1) that contains the aza-Asn epoxide and the P2 Pro of the first generation AOMK probe, as well as a Cy5 fluorophore for *in vivo* imaging applications (Figure 1, panel a). We also synthesized a Cy5-labeled version of the previously reported probe Biotin-PD-AOMK (LP-0, Figure 1, panel a) for direct comparison with LP-1. LP-1 was synthesized *via* a previously reported solid-phase synthesis technique (*20*), and the Cy5 fluorophore was conjugated to the purified peptide at the final step (Scheme 1). To directly compare enzyme specificity and kinetics between LP-1 and the previously described AOMKs, we also synthesized acetyl-capped inhibitor versions of LP-1 and LP-0 (LI-1 and LI-0, respectively; Figure 1, panel a).

**Selectivity and Potency of Legumain Inhibitors and Probes.** To determine the overall potency and selectivity of the aza-epoxide and AOMK inhibitors, we performed inhibition studies for both compounds against recombinant legumain, cathepsin B, cathepsin L, and caspase-3 (Table 1). Simple $IC_{50}$ determination showed that LI-1 ($IC_{50}$ = 11.5 nM) is 70-fold more potent than LI-0 ($IC_{50}$ = 704 nM) against legumain, whereas both compounds showed very weak activity against cathepsin B ($IC_{50}$ = 390 μM for LI-1 and >1 mM for LI-0) and cathepsin L ($IC_{50}$ = 220 μM for LI-1 and >1 mM for LI-0). Importantly, LI-0 showed a significant inhibitory effect ($IC_{50}$ = 2.8 μM) on caspase-3, whereas LI-1 showed nearly no inhibition ($IC_{50}$ = 890 μM). To further evaluate the kinetics of inhibition of legumain by the two classes of inhibitors, we also measured second-order rate constants ($k_{obs}/[I]$) for both compounds (Table 1). As expected, LI-1 ($k_{obs}/[I] = 72{,}352\ M^{-1}\ s^{-1}$) inhibited legumain approximately 50-fold faster than LI-0 ($k_{obs}/[I] = 1586\ M^{-1}\ s^{-1}$). These results confirmed that incorporation of P1 Asn *via* an aza-peptidyl scaffold greatly enhanced efficiency and specificity of inhibition by LI-1 compared to that of the P1 Asp AOMK scaffold. The rapid inhibition kinetics of the aza-Asn epoxide scaffold is advantageous for *in vivo* imaging as it allows

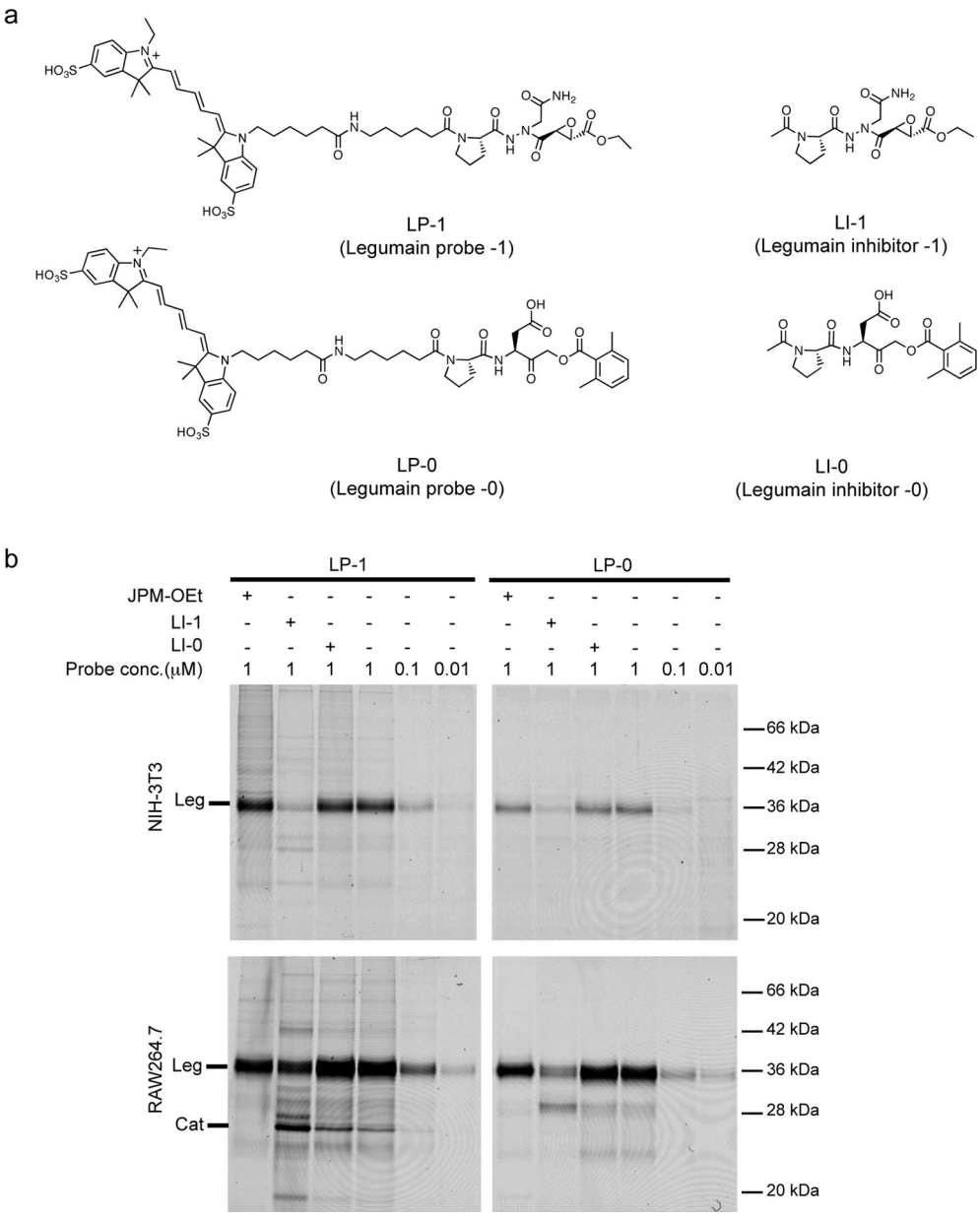


**Figure 1. Legumain inhibitors and probes. a) Structures of Aza-Asn epoxide legumain inhibitor, LI-1, and legumain probe, LP-1, compared to Asp-AOMK inhibitor, LI-0, and probe, LP-0. b) Direct labeling of legumain in intact cells by LP-1 and LP-0. Intact monolayers of NIH-3T3 fibroblasts (top) or RAW 264.7 macrophages (bottom) were pretreated with the cathepsin inhibitor JPM-OEt (10 μM; first column) and the legumain inhibitors LI-0/LI-1 (10 μM; second and third columns) and labeled by addition of LP-1 and LP-0 at the indicated concentrations.**

rapid binding to legumain, thus providing a better signal-to-noise ratio even for probes with relatively short half-lives *in vivo*. This allows the use of lower overall doses of probe and prevents extended circulation that can possibly cause cross-reactivity with other proteases.

**SCHEME 1. Synthesis of LP-1 and LI-1**

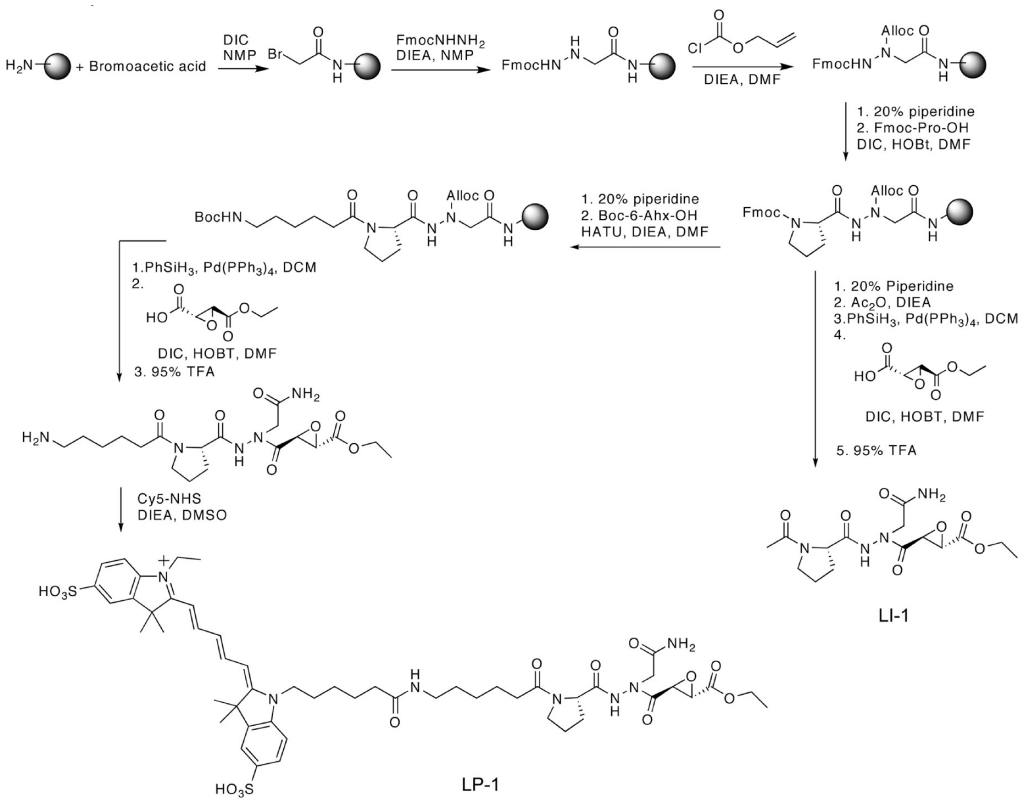


We next wanted to verify labeling of active legumain in intact cells. Therefore, we treated intact NIH-3T3 and RAW 264.7 cells with LP-1 and LP-0, respectively, and monitored protein labeling using SDS—PAGE followed by scanning of the gel to detect the Cy5 fluorescence (Figure 1, panel b). Both probes selectively labeled active legumain in NIH-3T3 fibroblasts. As previously observed in the enzyme kinetic assays, LP-1 labeled active legumain more efficiently than LP-0 at low probe concentrations and showed overall stronger labeling signals. Interestingly, when the two probes were used to label RAW 264.7 macrophages, both showed some degree of cross-reactivity toward lysosomal cathepsins. The identity of these off targets as cathepsins was con-

**TABLE 1. Inhibition of various cysteine proteases by LI-1 and LI-0**

| | Legumain | | | | |
|---|---|---|---|---|---|
| **Inhibitor** | **$IC_{50}$** | **$k_{obs}/[I]$** | **Cathepsin B $IC_{50}$** | **Cathepsin L $IC_{50}$** | **Caspase-3 $IC_{50}$** |
| LI-1 | 11.5nM | 72352 $M^{-1}$ $s^{-1}$ | 390 μM | 220 μM | 890 μM |
| LI-0 | 704 nM | 1586 $M^{-1}$ $s^{-1}$ | >1 mM | >1 mM | 2.8 μM |
| JPM-OEt[a] | | N/D | 0.78 μM | 2.98 μM | N/D |
| Z-DEVD-FMK[b] | | N/D | N/D | N/D | 0.13 μM |

[a]JPM-OEt is a broad-spectrum cathepsin inhibitor. [b]Z-DEVD-FMK is a caspase-3 specific inhibitor.

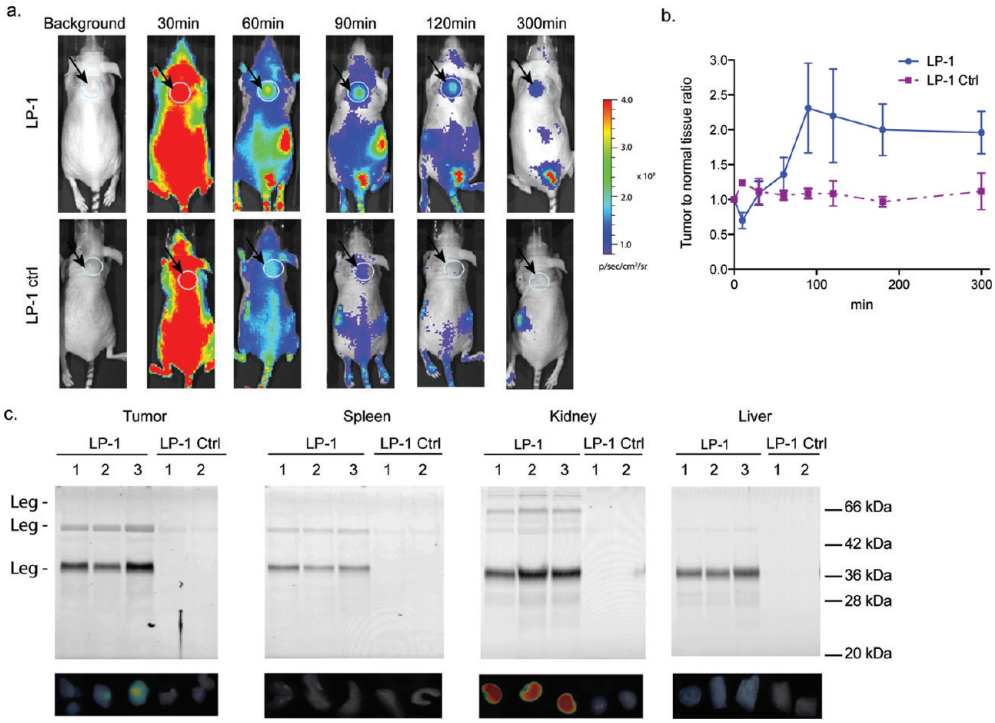


**Figure 2. Optical imaging of tumors in live mice and biochemical analysis of *in vivo* labeled legumain using LP-1. a) *In vivo* imaging of active legumain. Mice bearing C2C12/ras xenograft tumors were IV injected with LP-1 (top) or LP-1-ctrl (bottom) probes and imaged at the indicated time points. Images are presented using a colorimetric scale based on photons per second per centimeter square per steradian (p $s^{-1}$ $cm^{-2}$ $sr^{-1}$) overlaid on bright light images. b) Tumor to normal tissue signal ratio calculated from the mice labeled with LP-1 (circle symbols with a solid line) and LP-1 Ctrl (square symbols with a dotted line). Ratios were calculated from multiple mice ($n = 3$ for LP-1 and $n = 2$ for LP-1 Ctrl) and represent mean ± standard error. c) *Ex vivo* imaging of organs and protein labeling analyzed by SDS−PAGE. Fluorecently labeled proteins were visulaized by scanning of the gel using a flatbed laser scanner. Each column represents an organ from an individual mouse collected after *in vivo* imaging experiments.**

firmed by pretreatment of cells with the broad-spectrum cathepsin inhibitor JPM-OEt (*21*) and further verified by immunoprecipitation (Supplementary Figure S1). Although some degree of cross-reactivity of AOMK probes toward cathepsins has been reported (*15*), attempts to inhibit cathepsins with various aza-epoxide inhibitors have been unsuccessful (*22*). Therefore, the labeling of cathepsins by LP-1 was particularly surprising. These data suggest that even though compounds may have very low potency toward a particular protease target *in vitro*, when added to cells that actively accumulate the probes in their lysosomes, such as macrophages, they are able to react with other abundant proteases. Furthermore, when cells were pretreated with legumain inhibitors, we observed more intense cathepsin labeling. This could be explained by the fact that cathepsins are known to be substrates for legumain (*3, 23*); legumain inhibition thus could result in increased levels of cathepsins and therefore increased nonspecific labeling by the legumain probes. Although the cathepsin cross-reactivity is not ideal, by using lower probe concentrations and more potent inhibitor scaffolds, it should be possible to obtain selective labeling of legumain *in vivo*. On the basis of these results, we decided that LP-1 would be the optimal reagent for *in vivo* imaging studies, as it has faster kinetics and overall higher potency, resulting in less background labeling of cathepsins and caspases.

***In Vivo* Imaging of Legumain Using the Aza-Epoxide Probe LP-1.** To examine *in vivo* properties of LP-1 and monitor active legumain levels noninvasively, we performed imaging experiments using a simple tumor xe-

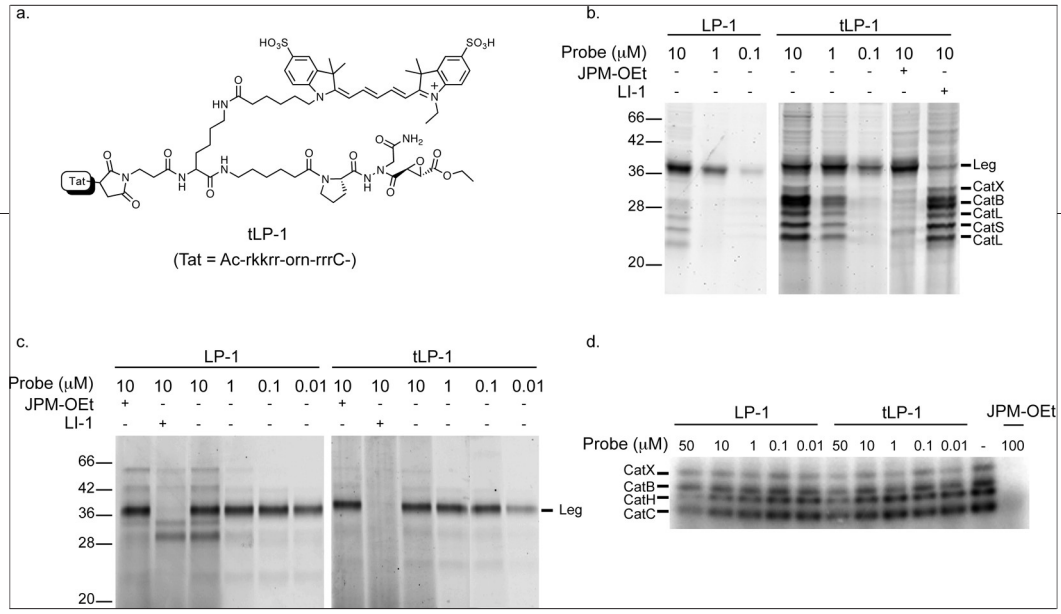


**Figure 3. Structure and labeling selectivity of tLP-1 intact cells. a) Structure of tat-conjugated LP-1 (tLP-1). b) Direct labeling of legumain in intact RAW 264.7 macrophages with LP-1 and tLP-1. Due to the differences in molecular weight between the two probes (approximately 1800), tLP-1 labeled legumain is slightly shifted on the gel relative to LP-1 labeled legumain. Where indicated, cells were pretreated with either the general cathepsin inhibitor JPM-OEt or the legumain-specific inhibitor LI-1. c) Comparison of labeling of legumain in RAW cell lysates by LP-1 and tLP-1. d) Competitive inhibition of cathepsins by LP-1 and tLP-1. RAW cell lysates were pretreated with LP-1 and tLP-1 at the indicated concentrations and labeled by the general cathepsin probe $^{125}$I-DCG04.**

nograft model (C2C12/Hras1) (*24*). To verify that the *in vivo* fluorescent signal from LP-1 is legumain-specific, we also used a control probe (LP-1 ctrl, see Supporting Information) that lacks the reactive epoxide group and therefore does not covalently bind to legumain. Mice were injected with the probes *via* tail vein, and fluorescent images were collected over the course of 5 h. As expected, LP-1 rapidly accumulated in tumor tissues, whereas LP-1 ctrl did not show such accumulation (Figure 2, panel a). Quantification of the tumor to normal tissue ratio from the fluorescent images showed that LP-1 accumulated in tumors with a maximum signal to background ratio obtained at around 90 min (Figure 2, panel b). Furthermore, the specific legumain signal declined over time but remained significantly higher than the signal observed for the control probe even at the later time points. This labeling pattern is in contrast to the previously reported cathepsin probes, which only provide contrast after 8−12 h, and signals are retained beyond 48 h. These data suggest that legumain may have a more rapid rate of turnover than the cathepsins and that the legumain probes have faster binding and clearance properties that lead to a more rapid signal over background.

At the end of the imaging time-course, we collected organs and carried out *ex vivo* imaging and SDS−PAGE analysis of extracts to confirm selective labeling of legumain by LP-1 (Figure 2, panel c). Importantly, fluorescent images of each tissue showed that levels of active legumain directly correlated with the intensity of legumain labeling as measured by SDS−PAGE analysis. The result also demonstrated that LP-1 is remarkably selective toward legumain *in vivo* and showed virtually no off-target labeling. These data further support our hypothesis that using a more potent and kinetically fast binding scaffold allows selective labeling of legumain *in vivo*.

**Use of a tat Peptide To Increase Cellular Uptake.** Previously we reported that conjugating the tat peptide to an activity-based probe that targets caspases enhanced cell permeability; however, it also increased lysosomal uptake due to its positive charge. Thus the use of the tat carrier inadvertently increased cross-reactivity toward legumain (*18*). Inspired by this result, we conjugated the tat peptide to LP-1 to further improve its *in vitro* and *in vivo* reactivity toward legumain. To our surprise, when tested against intact RAW 264.7 macrophages, tat conjugated LP-1 (tLP-1; Figure 3, panel a) labeled not only legumain but also multiple cathepsins, even at low concentrations (Figure 3, panel b). We believe that this cross-reactivity results from increased lysosomal uptake and is not the result of a loss of specificity caused by addition of the tat peptide. To test this hypothesis, we labeled RAW cell lysates with LP-1 and tLP-1 (Figure 3, panel c). SDS−PAGE analysis confirmed that there is no difference in reactivity toward legumain for these two probes. We also performed a competition assay by pretreating RAW lysates with each probe and labeling with the general cathepsin probe, I$^{125}$-DCG04 (*25*). These results further confirmed that both LP-1 and tLP-1 are equally poor inhibitors of the cathepsins (Figure 3, panel d). Thus, the increased cross-reactivity toward

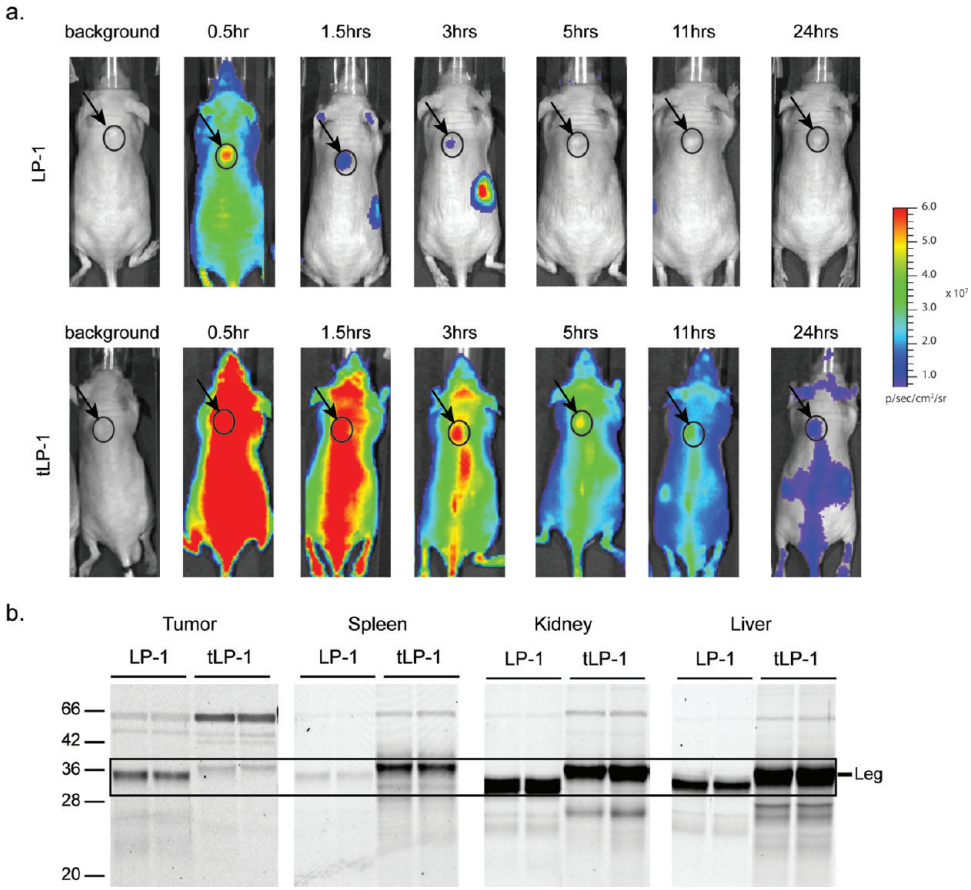


**Figure 4. Direct comparison of LP-1 and tLP-1 *in vivo*. a) *In vivo* imaging of legumain using LP-1 and tLP-1. Mice bearing C2C12/ras xenograft tumors were IV injected with LP-1 (top) or tLP-1 (bottom) probes and imaged at the indicated time points. Images are presented using a colorimetric scale based on photons per second per centimeter square per steradian (p $s^{-1}$ $cm^{-2}$ $sr^{-1}$) overlaid on bright light images. b) Biochemical characterization of *in vivo* labeled legumain. Fluorecently labeled proteins from tissue homogenates were visulaized by scanning of the gel using a flatbed laser scanner. Each column represents an organ from an individual mouse collected after *in vivo* imaging experiments.**

cathepsins is likely due to significant accumulation of tLP-1 in the lysosome.

Since tLP-1 showed high cross-reactivity toward cathepsins in cells, we wanted to monitor its *in vivo* distribution and labeling kinetics compared to those of LP-1. We performed *in vivo* imaging and found that although the tat peptide enhanced overall uptake of the probe, tLP-1 failed to show the selective uptake in tumors observed for LP-1. In addition, the tat peptide dramatically increased overall probe distribution and reduced the rate of clearance (Figure 4, panel a). As a result, tLP-1 showed increased nonselective labeling *in vivo* relative to that of LP-1 (Figure 4, panel b).

**Use of Additional Carrier-Conjugates on Legumain Probes.** Cell-penetrating peptides (CPPs) and membrane-targeting moieties have proven to be useful delivery methods for various biological reagents (*26, 27*). In addition to the tat peptide, we also decided to test several additional carrier molecules with our legumain probes. We chose octa-arginine (r8) and penetratin because of their widespread use as carriers. We also chose cholesterol since it has high affinity for membrane raft domains and has been used to enhance membrane permeability (*28*) (Figure 5, panel a).

To compare differences in cell permeability and labeling efficiency between these probes, we treated intact

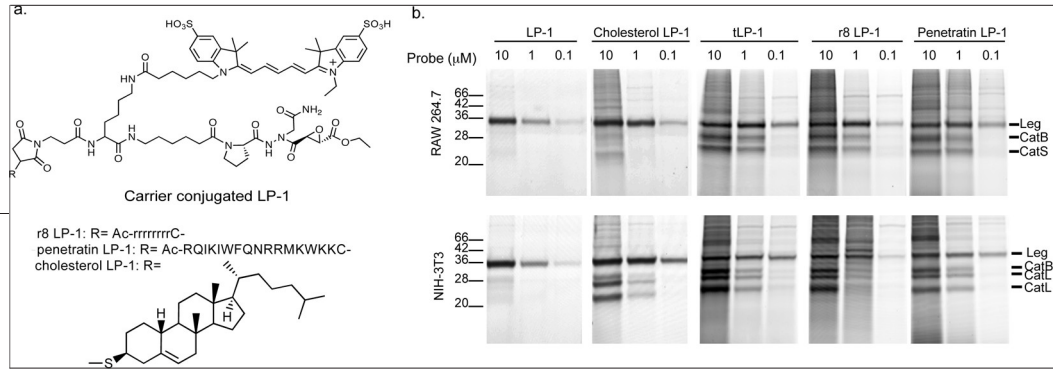


**Figure 5. Direct comparison between carrier-conjugated probes labeled in intact cells. a) Structures of the carrier-conjugated activity-based probes. b) Direct comparison between the carrier-conjugates. Intact RAW 264.7 macrophages (top) and NIH-3T3 fibroblasts (bottom) were labeled with each probe at the indicated concentrations. Total probe-labeled proteins were visualized by SDS−PAGE followed by scanning of the gel using a flatbed laser scanner. The locations of legumain (Leg) and cathepsins (Cat) are indicated.**

cells with each conjugate and analyzed labeling by SDS−PAGE. As previously observed for tLP-1, all the carrier-conjugates showed increased cellular uptake resulting in stronger labeling but also more cross-reactivity (Figure 5, panel b). All CPP conjugated probes, tLP-1, r8 LP-1, and penetratin LP-1 showed almost identical protein labeling profiles, indicating that all of these probes are delivered by similar mechanisms and are enriched in lysosomes. Cholesterol LP-1 showed enhanced legumain labeling with less cross-reactivity, suggesting that membrane anchoring cholesterol helped selective delivery of LP-1. Next, we carried out *in vivo* imaging experiments with penetratin LP-1 and cholesterol LP-1 to compare their *in vivo* distribution to LP-1 (Figure 6, panel a). Although the carrier labeled probes accumulated in tumors to some extent, their slow clearance resulted in low tumor to background levels (Figure 6, panel b). *Ex vivo* imaging of the collected organs followed by analysis of lysates by SDS−PAGE confirmed that carrier labeled probes suffered from increased cross-reactivity with cathepsin proteases (Figure 6, panel c). Overall, LP-1 showed the most legumain labeling in tumors as well as the highest levels of legumain-specific fluorescent signal, whereas penetratin LP-1 and cholesterol LP-1 showed nonspecific distribution in most organs and much higher cross-reactivity toward cathepsins. We believe that enhanced cellular delivery of these probes adversely affects overall circulation of the probe, resulting in less useful imaging reagents. Furthermore, all of the carrier molecules caused increased association with tissues other than the target tumors, suggesting that legumain ABPs are more effective as free probes that do not contain a carrier peptide.

In conclusion, we have developed a NIRF-labeled legumain probe, LP-1, based on a highly potent and selective inhibitor. The probe contains a Pro-Asn-aza epoxide scaffold that is distinct from the previously reported legumain inhibitors. When LP-1 was used for noninvasive imaging applications, we were able to monitor legumain activity both in normal tissues and in solid tumors. Its favorable reactivity and clearance resulted in high contrast in tumors soon after probe injection. We were also able to track whole body distribution of the probe as well as the level of active legumain in organs by *ex vivo* imaging and SDS−PAGE. In addition, we tested a series of cell-permeabilizing moieties as a delivery strategy for ABPs. Although some of these moieties improved cell permeability and legumain labeling in cells, they also increased off-target labeling *via* enhanced lysosomal uptake and extended circulation times *in vivo*. We conclude that LP-1 is a valuable new imaging probe with desirable *in vitro* and *in vivo* characteristics. While this probe can be used for noninvasive imaging studies, it also has great potential value for invasive applications in which direct assessment of levels of active legumain in whole tissues or cells *in vivo* are required. This new imaging agent and its corresponding inhibitor are likely to prove valuable for future *in vivo* studies of legumain function.

## METHODS

**General Methods.** Unless otherwise noted, all resins and reagents were obtained from commercial suppliers and used without further purification. All solvents used were HPLC-grade and also purchased from commercial suppliers. Reactions were analyzed by LC-MS performed on an Agilent 1100 liquid chromatography system with an API 150EX single quadrupole mass spectrometer (Applied Biosystems). HPLC purifications were carried out using an ÄKTA explorer 100 (Amersham Pharmacia Biotech) with $C_{18}$ reversed-phase columns (Waters). Mobile phase consisted of 95:5:0.1 = water/acetonitrile/trifluoroacetic acid (solvent A) and 0.1% trifluoroacetic acid in acetonitrile (solvent B). High-resolution mass spectrometry (HRMS) was performed using an LTQ-FTMS (Thermo Fisher Scientific). Matrix-assisted laser desorption ionization time-of-flight (MALDI-TOF) mass spectrometry was performed using a Bruker Autoflex TOF/TOF mass spectrometer (Bruker). $IC_{50}$ measurements and enzyme kinetics assays were performed on a Spectramax M5 fluorescent plate reader (Molecular Devices). Fluorescent gels were scanned with

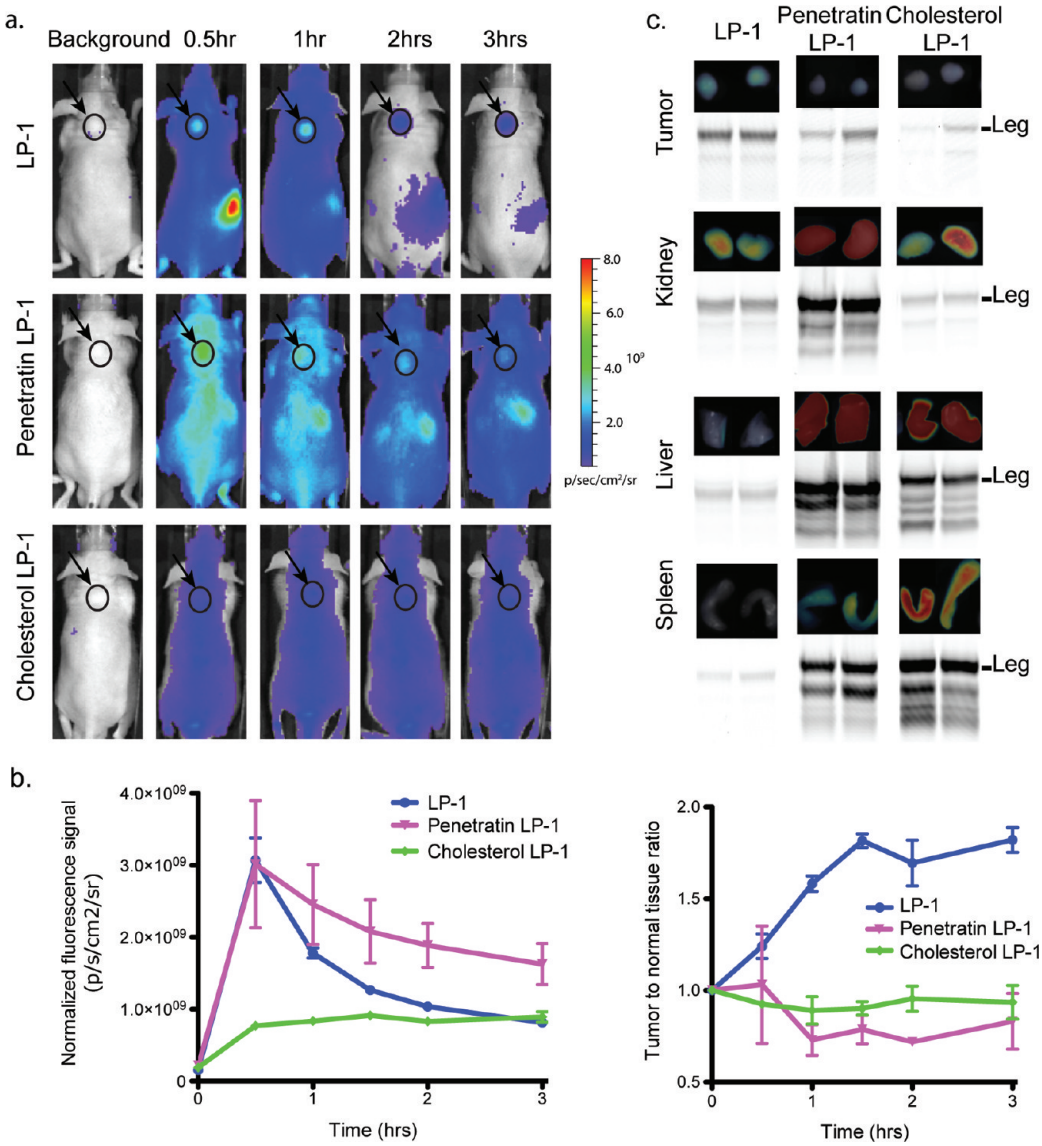


**Figure 6. *In vivo* imaging and biochemical analysis using penetratin LP-1 and cholesterol LP-1. a) Comparison of *in vivo* fluorescent images of mice labeled with LP-1 and carrier-conjugated probes. Mice bearing C2C12/ras xenograft tumors were IV injected with LP-1 (top) or Penetratin LP-1 (middle) and Cholesterol LP-1 (bottom) probes and imaged at the indicated time points. Images are presented using a colorimetric scale based on photons per second per centimeter square per steradian (p $s^{-1}$ $cm^{-2}$ $sr^{-1}$) overlaid on bright light images. b) *Ex vivo* imaging of whole organs and SDS–PAGE analysis from the corresponding organ extracts. Fluorecent probe labeled proteins were visualized by scanning of the gel using a flatbed laser scanner. The location of legumain (Leg) is shown. c) Quantification of fluorescent signal in tumors (left) compared to tumor to normal tissue signal ratios (right).**

a Typhoon 9400 flatbed laser scanner (GE Healthcare). Male BALB/c nude mice (4–8 weeks old) were obtained from Charles River and housed in the research animal facility at the Stanford University Department of Comparative Medicine. All animal protocols were approved by the Stanford Administrative Panel on Laboratory Animal Care, and the procedures were performed in accordance to their guidelines. *In vivo* imaging experiments were performed using the IVIS 200 imaging system (Xenogen), and *ex vivo* imaging experiments were performed using the FMT 2500 system (VisEn Medical).

**Synthesis and Characterization.** Peptidyl Aza-Asn epoxide was synthesized by following the previously reported procedure (*20*) on a Rink SS resin (Advanced ChemTech). Peptidyl Asp AOMK was synthesized by the previously reported procedure (*15*). Each carrier-probe conjugate was synthesized by following the previously reported procedure (*18*). The tat peptide and the penetratin peptide were custom synthesized by the Stanford PAN peptide synthesis facility. All synthesized peptides were cleaved from resin by applying cleavage cocktail containing 95% TFA and purified by HPLC. The purified peptides were then coupled with Cy5-NHS (1 equiv) in DMSO with DIEA (5 equiv) for 1 h and purified by HPLC. The purity and identity of all compounds were assessed by LC-MS and HR-MS. Detailed synthetic procedures and characterization data of final compounds can be found in Supporting Information.

**Determination of $IC_{50}$ against Cysteine Proteases and Second-Order Rate Constants ($k_{obs}/[I]$) for Legumain.** Activity of legumain was measured with the fluorogenic substrate, Cbz-Ala-Ala-Asn-AMC (Anaspec), cathepsin B and cathepsin L were measured with Cbz-Phe-Arg-AMC (Bachem), and caspase-3 was measured with Caspase-3 Substrate VII (Calbiochem). Assay buffers consist of 20 mM citric acid, 60 mM disodium hydrogen orthophosphate, 1 mM EDTA, 0.1% CHAPS, 4 mM DTT, pH 5.8 for legumain; 50 mM dihydrogen sodium orthophosphate, 1 mM EDTA, 5 mM DTT, pH 6.25 for cathepsin B and cathepsin L; and 100 mM Tris, 0.1% CHAPS, 10% sucrose, 10 mM DTT, pH 7.4 for caspase-3. Concentrations of substrates during the measurement were 10 μM (legumain, cathepsin L, and caspase-3) and 50 μM (cathepsin B), and concentration of enzymes were 100 nM for cathepsin L and caspase-3, 270 nM for legumain, and 360 nM for cathepsin B. Each enzyme was incubated with inhibitor concentrations ranging from 1 nM to 1 mM in the presence of the substrates. The increase in fluorescence was continuously monitored every 30 s for 2.5 h with a Spectramax M5 fluorescent plate reader (Molecular Devices), and inhibition curves were recorded. $IC_{50}$ values were calculated by plotting the normalized enzyme activity against the inhibitor concentration at 60 min for legumain and at 30 min for caspase-3, cathepsin B, and cathepsin L using nonlinear regression analysis (GraphPad Prism). $IC_{50}$ values with known broad-spectrum cathepsin inhibitor (JPM-OEt) and caspase-3 inhibitor (Z-DEVD-FMK) were also measured for comparison. All measurements were performed in triplicate, and the average values were reported.

Second-order inhibition rate constants were determined by following the previously described method in the literature (*6*). The pseudo-first-order rate constants ($k_{obs}$) were obtained from plots of ln $\nu_t/\nu_0$ versus time where $\nu_0$ is the rate of hydrolysis of fluorogenic substrate and $\nu_t$ is the rate of hydrolysis of substrate in the presence of the inhibitor. The second-order inhibition rate constants were calculated using the following equation: second-order rate constant $= (k_{obs}/[I])(1 + [S]/K_m)$.

**Direct Labeling of Endogenous Legumain in Intact Cells and Cell Lysates.** RAW 264.7 cells (250,000 cells well$^{-1}$) and NIH-3T3 cells (200,000 cells well$^{-1}$) were seeded in a 24-well plate 24−30 h prior to labeling. Cells were pretreated with appropriate inhibitors for 1.5 h and labeled by addition of each probe for 1 h; the final DMSO concentration was maintained at <0.2%. Cells were washed with PBS buffer and lysed by addition of sample buffer. Crude lysates were collected and separated by 12.5% SDS−PAGE. Labeled proteins were analyzed by scanning the gel with a Typhoon flatbed laser scanner (ex 633nM/em 680nM). For lysates labeling, cytosolic lysates of RAW 264.7 cells were prepared as previously described (*29*). Lysates were diluted to 1 mg mL$^{-1}$ in 50 mM citrate phosphate buffer (pH 4.5), 0.1% CHAPS, 5 mM DTT and subjected to direct labeling. Lysates samples (25 μL) were pretreated with inhibitors for 30 min and labeled with probes for another 30 min. The labeled samples were separated by 12.5% SDS−PAGE and analyzed by scanning the gel with a Typhoon flatbed scanner.

***In Vivo*/*ex Vivo* Imaging and SDS−PAGE Analysis of Organ Lysates.** Tumor-bearing mice were prepared by following the previously described method (*24*). C2C12/Hras1 or MDA-MB 231 MFP cells ($2 \times 10^6$ cells mouse$^{-1}$) were injected subcutaneously in 4−8 week old male BALB/c nude mice. Fourteen days after transplantation, each probe (25 nmol in 100 μL of sterile PBS) was injected *via* the tail vein into tumor-bearing mice. Mice were imaged at various time points after injection using the IVIS 200 imaging system equipped with a Cy5.5 filter. Relative fluorescence of equal-sized areas of tumor and background were measured using Living Image software (Caliper life science). Upon finishing the last time point of imaging, mice were anesthetized and sacrificed by cervical dislocation. Tumors, livers, kidneys, and spleens were collected and imaged *ex vivo* by using the FMT 2500 with a Cy5 filter. After *ex vivo* imaging, organs were lysed by a dounce homogenizer in muscle lysis buffer (1% Triton X-100, 0.1% SDS, 0.5% sodium deoxycholate, 0.2% sodium azide in PBS, pH 7.2). Total protein extracts (100 μg each) were separated by SDS−PAGE and visualized by scanning the gel with a Typhoon flatbed laser scanner.

*Acknowledgment:* We thank G. Blum and L. Edgington for valuable advice and technical assistance for initial animal experiments. We thank S. Verhelst and V. Albrow for helpful discussions about chemical synthesis. We also thank E. Deu Sandoval for help with enzyme assays, A. Guzzetta for HR-MS analysis, and F. Yin and M. Paulick for helpful discussions about cathepsins and assistance with the immunoprecipitations. This work was supported by a National Institutes of Health National Technology Center for Networks and Pathways grant U54 RR020843 (to M.B.), NIH grant R01-EB005011 (to M.B.).

*Supporting Information Available:* This material is available free of charge *via* the Internet at http://pubs.acs.org.

## REFERENCES

1. Ishii, S. (1994) Legumain: asparaginyl endopeptidase, *Methods Enzymol. 244*, 604–615.
2. Manoury, B., Mazzeo, D., Li, D. N., Billson, J., Loak, K., Benaroch, P., and Watts, C. (2003) Asparagine endopeptidase can initiate the removal of the MHC class II invariant chain chaperone, *Immunity 18*, 489–498.
3. Maehr, R., Hang, H. C., Mintern, J. D., Kim, Y. M., Cuvillier, A., Nishimura, M., Yamada, K., Shirahama-Noda, K., Hara-Nishimura, I., and Ploegh, H. L. (2005) Asparagine endopeptidase is not essential for class II MHC antigen presentation but is required for processing of cathepsin L in mice, *J. Immunol. 174*, 7066–7074.
4. Morita, Y., Araki, H., Sugimoto, T., Takeuchi, K., Yamane, T., Maeda, T., Yamamoto, Y., Nishi, K., Asano, M., Shirahama-Noda, K., Nishimura, M., Uzu, T., Hara-Nishimura, I., Koya, D., Kashiwagi, A., and Ohkubo, I. (2007) Legumain/asparaginyl endopeptidase controls extracellular matrix remodeling through the degradation of fibronectin in mouse renal proximal tubular cells, *FEBS Lett. 581*, 1417–1424.
5. Sottile, J., and Hocking, D. C. (2002) Fibronectin polymerization regulates the composition and stability of extracellular matrix fibrils and cell-matrix adhesions, *Mol. Biol. Cell 13*, 3546–3559.
6. Gotz, M. G., James, K. E., Hansell, E., Dvorak, J., Seshaadri, A., Sojka, D., Kopacek, P., McKerrow, J. H., Caffrey, C. R., and Powers, J. C. (2008) Aza-peptidyl Michael acceptors. A new class of potent and selective inhibitors of asparaginyl endopeptidases (legumains) from evolutionarily diverse pathogens, *J. Med. Chem. 51*, 2816–2832.

7. James, K. E., Gotz, M. G., Caffrey, C. R., Hansell, E., Carter, W., Barrett, A. J., McKerrow, J. H., and Powers, J. C. (2003) Aza-peptide epoxides: potent and selective inhibitors of *Schistosoma mansoni* and pig kidney legumains (asparaginyl endopeptidases), *Biol. Chem. 384*, 1613–1618.
8. Clerin, V., Shih, H. H., Deng, N., Hebert, G., Resmini, C., Shields, K. M., Feldman, J. L., Winkler, A., Albert, L., Maganti, V., Wong, A., Paulsen, J. E., Keith, J. C., Jr., Vlasuk, G. P., and Pittman, D. D. (2008) Expression of the cysteine protease legumain in vascular lesions and functional implications in atherogenesis, *Atherosclerosis 201*, 53–66.
9. Liu, C., Sun, C., Huang, H., Janda, K., and Edgington, T. (2003) Overexpression of legumain in tumors is significant for invasion/metastasis and a candidate enzymatic target for prodrug therapy, *Cancer Res. 63*, 2957–2964.
10. Luo, Y., Zhou, H., Krueger, J., Kaplan, C., Lee, S. H., Dolman, C., Markowitz, D., Wu, W., Liu, C., Reisfeld, R. A., and Xiang, R. (2006) Targeting tumor-associated macrophages as a novel strategy against breast cancer, *J. Clin. Invest. 116*, 2132–2141.
11. Chan, C. B., Abe, M., Hashimoto, N., Hao, C., Williams, I. R., Liu, X., Nakao, S., Yamamoto, A., Zheng, C., Henter, J. I., Meeths, M., Nordenskjold, M., Li, S. Y., Hara-Nishimura, I., Asano, M., and Ye, K. (2009) Mice lacking asparaginyl endopeptidase develop disorders resembling hemophagocytic syndrome, *Proc. Natl. Acad. Sci. U.S.A. 106*, 468–473.
12. Kembhavi, A. A., Buttle, D. J., Knight, C. G., and Barrett, A. J. (1993) The two cysteine endopeptidases of legume seeds: purification and characterization by use of specific fluorometric assays, *Arch. Biochem. Biophys. 303*, 208–213.
13. Niestroj, A. J., Feussner, K., Heiser, U., Dando, P. M., Barrett, A., Gerhartz, B., and Demuth, H. U. (2002) Inhibition of mammalian legumain by Michael acceptors and AzaAsn-halomethylketones, *Biol. Chem. 383*, 1205–1214.
14. Sexton, K. B., Witte, M. D., Blum, G., and Bogyo, M. (2007) Design of cell-permeable, fluorescent activity-based probes for the lysosomal cysteine protease asparaginyl endopeptidase (AEP)/legumain, *Bioorg. Med. Chem. Lett. 17*, 649–653.
15. Kato, D., Boatright, K. M., Berger, A. B., Nazif, T., Blum, G., Ryan, C., Chehade, K. A., Salvesen, G. S., and Bogyo, M. (2005) Activity-based probes that target diverse cysteine protease families, *Nat. Chem. Biol. 1*, 33–38.
16. Rozman-Pungercar, J., Kopitar-Jerala, N., Bogyo, M., Turk, D., Vasiljeva, O., Stefe, I., Vandenabeele, P., Bromme, D., Puizdar, V., Fonovic, M., Trstenjak-Prebanda, M., Dolenc, I., Turk, V., and Turk, B. (2003) Inhibition of papain-like cysteine proteases and legumain by caspase-specific inhibitors: when reaction mechanism is more important than specificity, *Cell Death Differ. 10*, 881–888.
17. Loak, K., Li, D. N., Manoury, B., Billson, J., Morton, F., Hewitt, E., and Watts, C. (2003) Novel cell-permeable acyloxymethylketone inhibitors of asparaginyl endopeptidase, *Biol. Chem. 384*, 1239–1246.
18. Edgington, L. E., Berger, A. B., Blum, G., Albrow, V. E., Paulick, M. G., Lineberry, N., and Bogyo, M. (2009) Noninvasive optical imaging of apoptosis by caspase-targeted activity-based probes, *Nat. Med. 15*, 967–973.
19. Berger, A. B., Witte, M. D., Denault, J. B., Sadaghiani, A. M., Sexton, K. M., Salvesen, G. S., and Bogyo, M. (2006) Identification of early intermediates of caspase activation using selective inhibitors and activity-based probes, *Mol. Cell 23*, 509–521.
20. Kato, D., Verhelst, S. H., Sexton, K. B., and Bogyo, M. (2005) A general solid phase method for the preparation of diverse azapeptide probes directed against cysteine proteases, *Org. Lett. 7*, 5649–5652.
21. Joyce, J. A., Baruch, A., Chehade, K., Meyer-Morse, N., Giraudo, E., Tsai, F. Y., Greenbaum, D. C., Hager, J. H., Bogyo, M., and Hanahan, D. (2004) Cathepsin cysteine proteases are effectors of invasive growth and angiogenesis during multistage tumorigenesis, *Cancer Cell 5*, 443–453.
22. Asgian, J. L., James, K. E., Li, Z. Z., Carter, W., Barrett, A. J., Mikolajczyk, J., Salvesen, G. S., and Powers, J. C. (2002) Aza-peptide epoxides: a new class of inhibitors selective for clan CD cysteine proteases, *J. Med. Chem. 45*, 4958–4960.
23. Shirahama-Noda, K., Yamamoto, A., Sugihara, K., Hashimoto, N., Asano, M., Nishimura, M., and Hara-Nishimura, I. (2003) Biosynthetic processing of cathepsins and lysosomal degradation are abolished in asparaginyl endopeptidase-deficient mice, *J. Biol. Chem. 278*, 33194–33199.
24. Blum, G., von Degenfeld, G., Merchant, M. J., Blau, H. M., and Bogyo, M. (2007) Noninvasive optical imaging of cysteine protease activity using fluorescently quenched activity-based probes, *Nat. Chem. Biol. 3*, 668–677.
25. Lennon-Dumenil, A. M., Bakker, A. H., Maehr, R., Fiebiger, E., Overkleeft, H. S., Rosemblatt, M., Ploegh, H. L., and Lagaudriere-Gesbert, C. (2002) Analysis of protease activity in live antigen-presenting cells shows regulation of the phagosomal proteolytic contents during dendritic cell activation, *J. Exp. Med. 196*, 529–540.
26. Fischer, R., Fotin-Mleczek, M., Hufnagel, H., and Brock, R. (2005) Break on through to the other side-biophysics and cell biology shed light on cell-penetrating peptides, *ChemBioChem 6*, 2126–2142.
27. Mintzer, M. A., and Simanek, E. E. (2009) Nonviral vectors for gene delivery, *Chem. Rev. 109*, 259–302.
28. Rajendran, L., Schneider, A., Schlechtingen, G., Weidlich, S., Ries, J., Braxmeier, T., Schwille, P., Schulz, J. B., Schroeder, C., Simons, M., Jennings, G., Knolker, H. J., and Simons, K. (2008) Efficient inhibition of the Alzheimer's disease β-secretase by membrane targeting, *Science 320*, 520–523.
29. Sexton, K. B., Kato, D., Berger, A. B., Fonovic, M., Verhelst, S. H., and Bogyo, M. (2007) Specificity of aza-peptide electrophile activity-based probes of caspases, *Cell Death Differ. 14*, 727–732.